

Application of Decision Tree and Support Vector Machine for Inspecting Bubble Defects on LED Sealing Glue Images

* Chuan-Yu Chang and Yi-Feng Lin

Abstract

Bubble defect inspection is an important step in light-emitting diode (LED) packaging processes. It is difficult to detect bubble defects because bubbles are transparent and have irregular shapes in LED sealing glue images. Traditionally, experienced engineers visually check defect regions and exclude defective elements. However, the inspection processes are costly and time-consuming. This paper proposes an automatic bubble defect inspection method for LED sealing glue images. The system automatic locates the sealing glue region. A decision tree is adopted to outline regions of interest (ROI), and many textural and geometric features are extracted from the ROIs. A support-vector-machine (SVM) is used to classify the ROIs as acceptable or defective. Experimental results demonstrate effectiveness of the proposed approach.

Keywords: light-emitting diode, defect inspection, decision tree, support-vector-machine

1. Introduction

Since the invention of the lighting equipment, lighting has become an indispensable product. LED is a semiconductor device that emits visible light. Compared with traditional illuminating devices, the features of LED have smaller volume, lower power requirements, higher efficiency, and a longer lifetime.

Figure 1 shows a LED product and its component structure. There are many types of defects in the silicone encapsulant, such as short shot, flash, damage, and bubble. However, inspecting LED surface defects by human eyes is inefficient. In industrial manufacturing, most defects can be detected by using the automatic detection system.

There have been many methods proposed for defect inspection [1-4]. Li et al. applied a wavelet-based algorithm for the inspection of multicrystalline solar images [1]. They used the wavelet coefficients to distinguish local defects and also to enhance the discriminant features using the wavelet's energy differences in two consecutive decomposition levels. Liu et al. proposed a defect detection method based on two-dimensional discrete wavelet transformation [2]. The defects were detected by comparative reconstructed standard images and test images. This method alignment and structure affect the results. In addition, an incorrect standard wafer image may result in inspection mistakes. Li et al. proposed a level-set method for LED wafer inspection [3]. They utilized the zero-level contours for segmenting wafers. Defects were detected by textural and geometric features. However, they are rather complex and time-consuming processes. Chiou applied the decision tree to select a proper image segmentation method for detecting defects [4]. However, the proposed detection method is only suitable in a simple image.

*Corresponding Author: Chuan-Yu Chang
(E-mail: chuanyu@yuntech.edu.tw)

¹Department of Computer Science and Information Engineering,
National Yunlin University of Science and Technology, 123, Sec.3,
University Rd., Douliou, Yunlin, 640, Taiwan

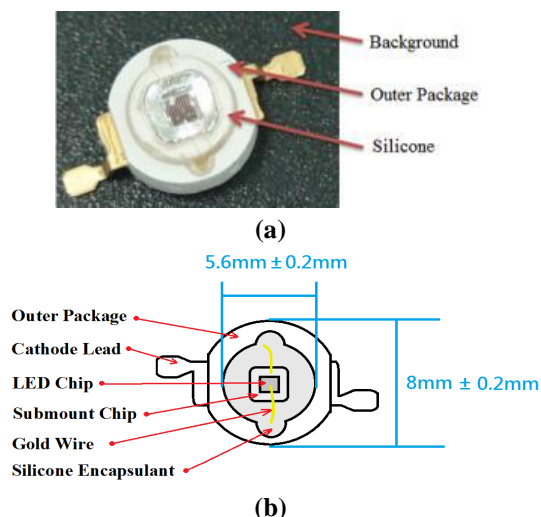


Figure 1: (a) LED product and (b) Basic LED structure.

Most methods are based on the analysis of the differences of textural and geometric features. Since LED sealing glue images have a large area to be inspected, a system requires a long time to calculate the textural features for each pixel. However, it is difficult to detect the limp and inconstant bubble defects. Therefore, this paper develops a method to detect bubble defects by geometric features in LED sealing glue images.

Since the LED silicone region is a smooth surface, it is important to build a single and uniform light source capture environment to reduce noises. Before applying the algorithm, first, the silicone encapsulant was segmented, which is a transparent layer on the LED structure. Next, decision tree is applied to analyze bubble, edge and background region to obtain the potential defect regions. The features of potential defect regions were extracted, and then these features are classified by the SVM. Finally, the positions of the bubble are represented.

This paper is organized as follows: In Section 2, the approach for LED bubble defect inspection is described, including preprocessing, ROI extraction, feature extraction, and classification. Section 3 demonstrates the experimental results. Finally, conclusions are given in Section 4.

2. Bubble Defect Inspection

Figure 2 shows the flowchart of the proposed method. There are four major steps in the proposed method. Details are described as follows:

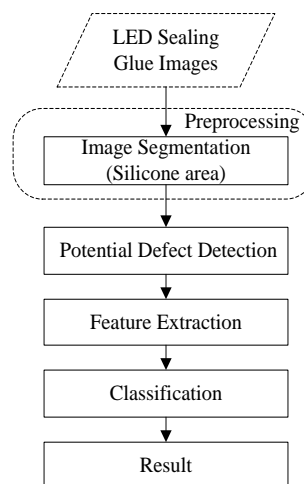


Figure 2: The flowchart of the proposed method

2.1 Preprocessing

As shown in Figure 1(a), a LED sealing glue image consists of three components: the background, the outer package region and the silicone region. Since bubble defects occur only in the silicone region, the purpose of the preprocessing is to segment the silicone region.

The brightness of an LED sealing glue image can be divided into two parts. The darker area is background; and the lighter area is LED. Therefore, Otsu's method is used to separate the LED sealing glue images into background and LED regions [5]. Otsu's method is capable of finding an optimal threshold value from the distribution of an image. The algorithm finds an optimal threshold value to divide a LED sealing glue image into two groups, while the sum of variances of the two groups is the minimum. The optimal threshold is defined as the weighted sum of variances of the two groups:

$$t_{opt} = \arg \min_t [w_1(t)\sigma_1(t) + w_2(t)\sigma_2(t)] \quad (1)$$

where w_1 and w_2 are the probabilities of the two groups separated by t ; σ_1 and σ_2 are the standard deviations of the two groups; $t \in [0, L]$, and L is the image level.

Figure 3(a) shows an original LED image. Figure 3(b) is the thresholding result by Otsu's method. Since the white regions in the segmented LED image are not connected to the background region, it is easy to extract the complete background region by means of connected-component labeling. Figure 3(c) shows the segmented background region. Based on the segmented LED region, we can obtain the centroid of LED. And then extract the outer package region. The outer package region is a donut-like circle with radius from 120 to 160 pixels. Figure 3(d) shows the centroid of the LED and the outer package region.

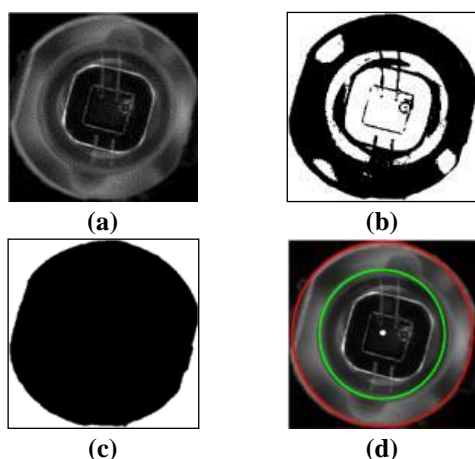


Figure 3: Background segmentation: (a) the original image; (b) result of Otsu's method; (c) detected background, and (d) LED centroid and outlined outer package region.

Since the silicone region cannot be determined by a threshold value, the adaptive thresholding method is adopted to segment silicone region. The adaptive thresholding method can suppress the influence of illumination [6]. The adaptive threshold value is computed as:

$$Ada_Th(x, y) = \frac{\sum_{i=-m/2}^{m/2} \sum_{j=-m/2}^{m/2} f(x+i, y+j)}{m \times m} \times t \quad (2)$$

where $f(x, y)$ is the gray intensity of pixel (x, y) .

If the pixel intensity is lower than the threshold value, then it is set to 0, otherwise it is set to 1; that is:

$$Out(x, y) = \begin{cases} 1 & , f(x, y) \geq Ada_Th(x, y) \\ 0 & , f(x, y) < Ada_Th(x, y) \end{cases} \quad (3)$$

Figure 4(a) shows the segmented regions by adaptive thresholding. In order to obtain completely segmentation results, a morphological closing operation with a 9×9 structuring element is applied. Then the resulting image is converted negatively as shown in Figure 4(b). Figure 4(c) shows the outer package region and parts of the silicone region. The two regions are not connected. Figure 4(d) is the negative of Figure 4(c), and it excludes the background region. A complete silicone region is obtained by removing the non-silicone region and filling holes. Figures 4(e) and 4(f) show the detected silicone region and the silicone region in the original image.

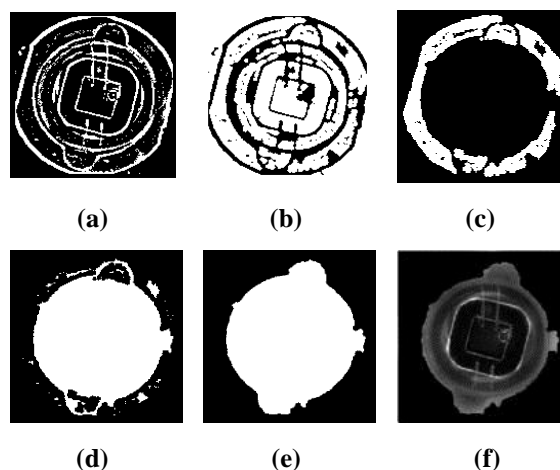


Figure 4: (a) Adaptive thresholding result (b) the negative of (a); (c) outer package regions; (d) the negative of (c); (e) the silicone region, and (f) the silicone region in original image.

2.2 Subjective Characteristics of Elderly Speech

The bubble defects are circular and transparent with different sizes. According to the property of bubbles, we can use the decision tree to classify them into three classes: 1) edge, 2) interior of bubble and 3) background.

A decision tree is a method to represent information by a machine learning algorithm [7]. All the training patterns are outlined manually by experienced engineers. Four features are then extracted by using a $n \times n$ sliding window from each training pattern:

- 1). $M(x, y)$: the mean of pixel intensity in the window.
- 2). $Std(x, y)$: the standard deviation of pixel intensity in the window.
- 3). $R(x, y)$: the ranked position of the center pixel in the window.
- 4). $FR(x, y)$: the red component of the center pixel in the window.

In the training phase, each class selected 900 patterns for training and 300 patterns for testing. After the training process, the decision tree model was obtained as shown in Figure 5. Figure 6 shows the classification results of Figure 4(f) by decision tree.

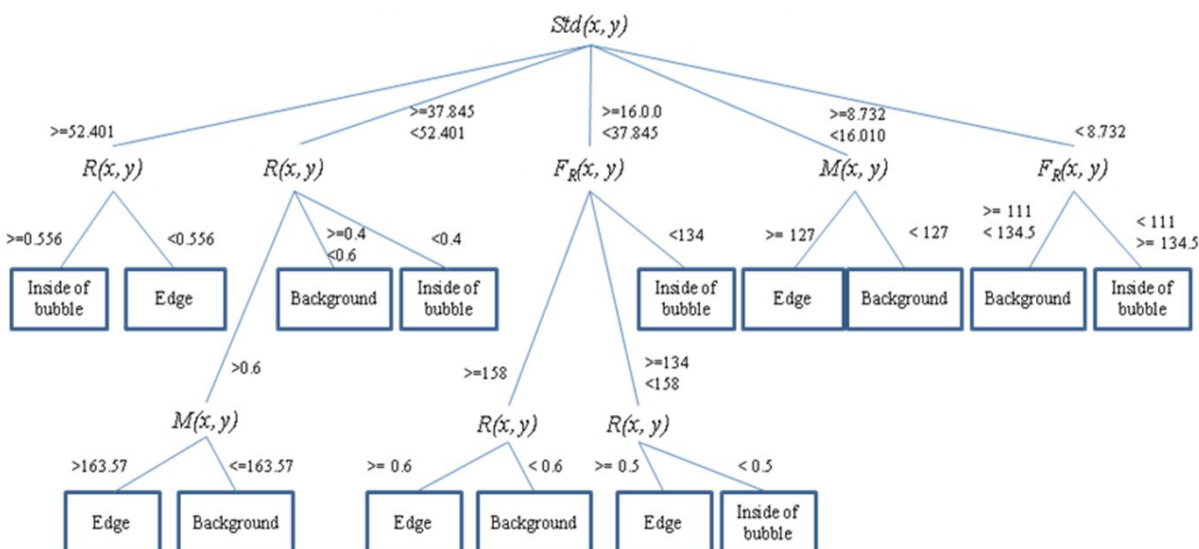


Figure 5: Result of decision tree

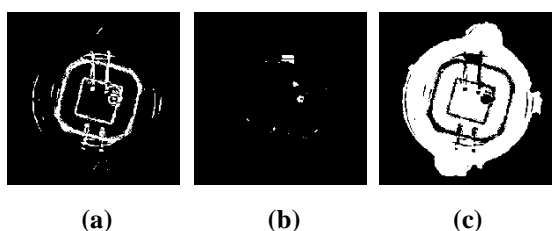


Figure 6: Classification of the silicone region: (a) the edge regions; (b) the interior of bubble regions and (c) the LED background regions.

By observing the interior of bubbles, we could exclude non-bubble defect regions. The minimum bounding rectangle (MBR) is the smallest rectangle which encloses potential defect regions completely. Yang proposed a fast calculation of a minimum area exterior rectangle method [8]. The method is used to determine the spindle, which is the inertia according to the rotary inertia of an object. MBR can be obtained by using image rotation with the edge and spindle of the object. Therefore, we eliminated the regions in which the MBR aspect ratio is greater than 2.5, and the length of a longer side is greater than 55 pixels.

Figure 7(a) shows the locations of potential defects, which had excluded non-bubble defect region. Therefore, the potential defect regions extracted correspond to these internal of bubble regions, as the green rectangles shown in Figure 7(b). The potential defect regions will be processed in next step.

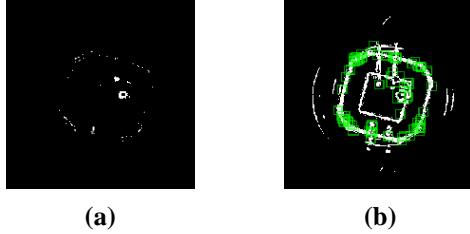


Figure 7: (a) Potential defects and (b) potential defect regions

2.3 Feature Extraction

The purpose of feature extraction is to obtain features to discriminate between defects and non-defects. In order to enhance performance of the identification, the potential defect regions are transformed to the polar coordinate system. The polar coordinates (r, θ) can be calculated from the Cartesian coordinates by:

$$r = \sqrt{(X_p - X_o)^2 + (Y_p - Y_o)^2}, \theta = \tan^{-1} \left(\frac{Y_p - Y_o}{X_p - X_o} \right) \quad (4)$$

where (X_o, Y_o) is the origin, (X_p, Y_p) is the position in the Cartesian coordinates.

Figures 8 (a2)-(d2) show the transformation results. The horizontal axis is the angle $[0, 2\pi]$, and the vertical axis is the radius distance. Obviously, the bubble defects and normal regions in a polar coordinates system are different.

In general, bubble defects have a similar appearance. Let P_H and P_V denote the horizontal projection ratio and vertical projection ratio, respectively. The P_H and P_V are defined as

$$P_H(\theta) = \frac{1}{N_r} \sum_{i=1}^R B(i, \theta) \quad , \text{for } \theta = 0, 1, \dots, 359 \quad (5)$$

$$P_V(i) = \frac{1}{N_r} \sum_{\theta=0}^{359} B(i, \theta) \quad , \text{for } i = 1, \dots, R \quad (6)$$

where $B(i, \theta)$ is the intensity at the polar coordinate (i, θ) , R is the length of radius, and N_r is the number of non-zero value in the transformed image B .

Since bubble defects are concentrated in a small range of the vertical projection. A factor P is calculated to evaluate the concentration of the vertical projection

$$P = \sum_{i=1}^R (P_V(i) | P_V(i) < \frac{250}{N_r}) \quad (7)$$

In general, the bubble defects have small value of P .

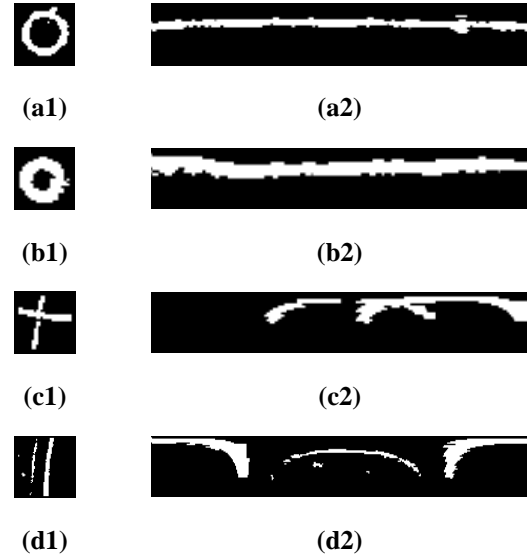


Figure 8: (a1)-(d1) Potential defect regions, and (a2)-(d2) Potential defect regions at the polar coordinate.

2.4 Inspection Algorithm

The similarity measurement was applied to compare the feature of horizontal projection ratio between two histograms. Three similarity measurements described below are calculated.

Chi-square distance,

$$d_c(H, H') = \sum_{i=0}^n \left(\frac{(H(i) - H'(i))^2}{H(i) + H'(i)} \right) \quad (8)$$

Bhattacharyya distance,

$$d_b(H, H') = \sqrt{1 - \sum_{i=0}^n (H(i) \times H'(i))^{\frac{1}{2}}} \quad (9)$$

Intersection ratio,

$$d_f(H, H') = \sum_{i=0}^n \text{Min}(H(i), H'(i)) \quad (10)$$

where H and H' denote the horizontal projection histogram of bubble template and potential defect region, respectively.

The three distances and factor P are aggregated as a feature vector as

$$\mathbf{v} = [d_C, d_B, d_I, P] \quad (11)$$

The SVM has been widely used in many pattern recognition problems [9,10]. It finds a hyperplane to classify patterns into two classes. Assume that a set of vectors D belongs to two separable classes,

$$\mathbf{D} = \{(\mathbf{v}_1, d_1), (\mathbf{v}_2, d_2), \dots, (\mathbf{v}_n, d_n)\}, d_i \in \{-1, +1\} \quad (12)$$

The hyperplane can be represented as

$$g(\mathbf{v}) = \text{sgn} \left(\sum_{i=1}^l \alpha_i d_i \exp \left(\frac{-\|\mathbf{v} - \mathbf{v}'_i\|^2}{2\sigma^2} \right) + b \right) \quad (13)$$

where α_i is the weight parameter, \mathbf{v}'_i is support vector, l is the number of support vectors, σ is bandwidth and b is a bias.

In the training phase, 60 training patterns, including 30 defect patterns and 30 non-defect patterns, are selected. The non-defect patterns were selected from potential defect regions. And the best model was selected by two-fold cross-validation. After the training phase, the SVM model can be obtained and processed. Figure 9 shows the structure of the SVM classifier for bubble defects classification.

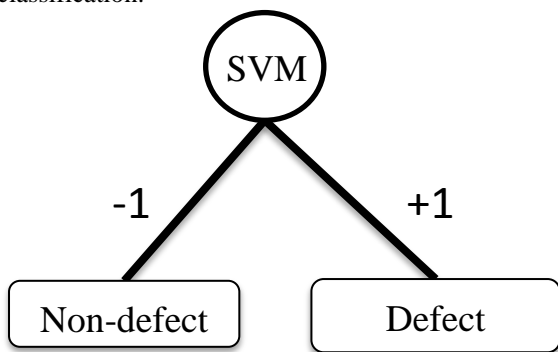


Figure 9: The structure of the SVM classifier.

3. Experimental Results

The proposed method was implemented by Microsoft Visual Studio 2008 C# on an Intel Core i7 3.4GHz processor with 4GB RAMs. There are two LED sealing glue image databases captured from different light sources (white and red) with the same LEDs. Each database contains 120 LED images including 75 images with bubble defects and 45 images without bubble defect. Figure 10 shows examples of the two databases. The average inspection time of the proposed method was 1.2s per image. Three experiments were conducted in this paper.

3.1 Potential Defect Detection Under Various Window Sizes

In the proposed method, potential defect regions were detected by decision tree. To find the best setting for window size, four sizes of window (3×3, 5×5, 7×7 and 9×9) were used for feature extraction. In this experiment, there exist 148 bubble defects in the 25 LED sealing glue images. Table 1 presents the experimental results under different window sizes. The result shows that the window with size of 7×7 can detect the most bubble defects. Four bubble defects were missed. These undetected bubble defects are usually blurred and insignificant with sizes less than 10×10 pixels. Therefore, the window with a size of 7×7 was selected in the subsequent experiments.

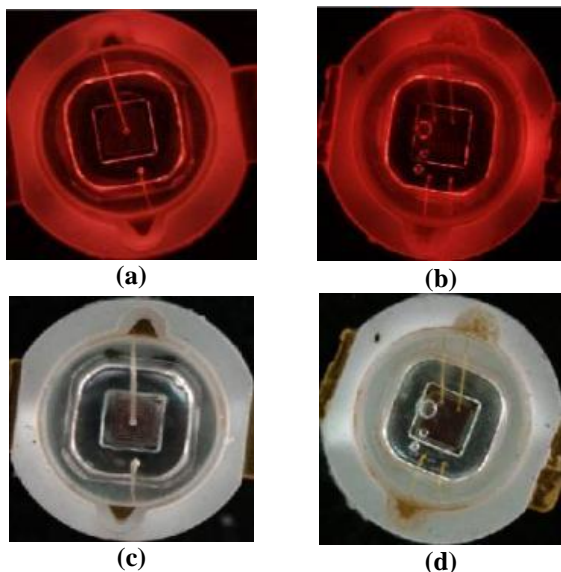


Figure 10: Example of LED sealing glue images:
 (a) Normal LED image captured from red light source; (b) Defective LED image captured from red light source; (c) Normal LED captured from white light source, and (d) Defective LED image captured from white light source.

Table 1: Potential defect detection result

Window size	# of potential bubble defects	# of undetected bubble defects
3×3	3253	62
5×5	4219	16
7×7	3759	4
9×9	3477	18

3.2. Bubble Defect Detection

In order to evaluate the performance of the proposed method, the sensitivity, specificity and accuracy were calculated. Assume N_p is the actual number of bubble defects. The N_n is the actual number of normal regions. N_{ip} is the number of actual defective regions that the system detects. And the N_m is the number of actual normal regions that the system detects. The sensitivity, specificity and accuracy are defined as follows.

$$Sensitivity = \frac{N_{ip}}{N_p} \tag{14}$$

$$Specificity = \frac{N_m}{N_n} \tag{15}$$

$$Accuracy = \frac{N_{ip} + N_m}{N_n + N_p} \tag{16}$$

80 LED images captured from white and red light sources were used for testing. Table 2 shows the bubble defect detection results under different lighting sources. The system detects more potential defect regions from the LED images captured from white light source. This factor causes the experiment to have high false positives and take longer time to detect defects. Table 3 presents the performance. These values demonstrate that the proposed method can detect bubble defects with high sensitivity. The result shows that the whole classification accuracy in red light is better than that in white light. Figure 11 shows the bubble defect detection results. Bubbles are outlined by rectangles, and the green rectangles outline the real bubbles; the blue rectangles are over detected defects. These false positive regions are usually located on the edge or shadow regions, as the blue rectangles shown in Figure 11(a). Figure 11(b) shows the results are more robust and accurate with red light sources.

Table 2: Confusion matrix of bubble defect detection.

Actual	Predicted	
	Defect	Normal
Red light source		
Defect	126	14
Normal	715	3915
White light source		
Defect	122	18
Normal	2456	6757

Table 3: Performance of defect detection.

Light source	Sensitivity	Specificity	Accuracy
Red	90.00%	84.58%	84.72%
White	87.14%	73.34%	73.55%

3.3 Compared with other methods

In the image, the bubble can extract shape features for identification. Since images use different segmentation methods to segment the bubble, the results of segmentation image are not the same. That could affect the efficiency of the identification results. This experiment used different segmentation algorithms to compare defect inspection. The popular edge detectors including Sobel and Canny edge detectors and Otsu's method were selected for comparison with the proposed approach.

Table 4 shows the performance comparison of four segmentation methods. There are 140 bubble defects and 4630 normal regions which are the potential defect regions in 40 LED sealing glue images. In the proposed method, the sensitivity and specificity is 0.9 and 0.85, respectively. Although Canny's method has a higher accuracy, its sensitivity is less than the proposed method, which means Canny's method cannot detect bubble defects accurately. As shown in Table 4, these values demonstrate that the effectiveness of the proposed method can efficiently inspect the bubble defects in the LED sealing glue images.

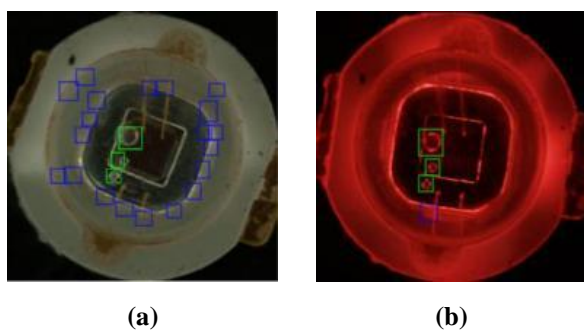


Figure 11: (a) the detected bubble defects from the white light source, and (b) the detected bubble defects from the red light source.

Table 4: Performance comparison of the four segmentation methods.

	Canny	Sobel	Otsu	Proposed
<i>Defect region</i>				
Defect	65	111	114	126
Normal	75	29	26	14
<i>Normal region</i>				
Defect	269	1032	987	715
Normal	4361	3598	3643	3915
Sensitivity	0.46	0.79	0.81	0.9
Specificity	0.94	0.78	0.79	0.85
Accuracy	0.92	0.78	0.79	0.85

4. Conclusions

LED can be produced quickly with automatic manufacturing systems. Automatic visual defect inspection plays an important role with the benefits of low-cost and high accuracy. This paper proposed a bubble defects detection scheme for LED sealing glue images. The silicone region was extracted so that the region needed to be inspected was reduced, and thus the defect regions were determined. The positions of potential bubble defects can be obtained by using decision tree. The SVM is applied to classify the potential defects into defect and non-defect. The experimental data show that LED sealing glue image in red light source has higher accuracy than in white source. The results show that the proposed method is effective to detect bubble defects on LED sealing glue images.

Acknowledgments

This work was supported by the National Science Council Taiwan, R.O.C, under the grants NSC 100-2218-E-244- 007.

References

- [1]. W.-C. Li, D.-M. Tsai, "Wavelet-based defect detection in solar wafer images with inhomogeneous texture," *Pattern Recognition*, vol. 45, pp. 742-756, 2011.
- [2]. H. Liu, W. Zhou, Q. Kuang, L. Cao, B. Gao, "Defect detection of IC wafer based on two-dimension wavelet transform," *Microelectronics Journal*, vol. 41, pp. 171-177, 2010.
- [3]. C.-H. Li, C.-Y. Chang, M.-D. Jeng, "Applying regional level-set formulation to post-sawing four-element LED wafer inspection," *IEEE Transactions on Systems, Man, and Cybernetics--Part C: Applications and Reviews*, vol. 41, no. 6, pp.842-853, Nov. 2011.
- [4]. Y.-C. Chiou, "Intelligent segmentation method for real-time defect inspection system," *Computers in Industry*, vol. 61, No. 7, pp. 646-658, 2010.
- [5]. N. Otsu, "A threshold selection method from gray-level histograms," *IEEE Transactions on Systems, Man and Cybernetics*, vol. 9, no. 1, pp. 62-66, Jan. 1979.
- [6]. D. Bradley and G. Roth, "Adaptive thresholding using the integral image," *Journal of Graphics Tools*, vol. 12, no. 2, pp. 13-21, 2007.
- [7]. Quinlan, J. R., *C4.5: Programs for Machine Learning*, Morgan Kaufmann Publishers, 1993.
- [8]. C. Yang, R. Lu, N. Chen, "A fast method for large aperture optical elements surface defects detection," *Advances in MSEC*, Vol. 2, pp. 175-184, 2011.
- [9]. C. C. Chang and C. J. Lin, *LIBSVM: a library for support vector machines*, 2001.
Available:
<http://www.csie.ntu.edu.tw/~cjlin/libsvm>.
- [10]. C. Cortes and V. Vapnik, "Support-vector network," *Machine Learning*, Vol. 20, pp. 273-297, 1995.



Chuan-Yu Chang received the Ph.D. degree in electrical engineering from National Cheng Kung University, Tainan, Taiwan, in 2000. He is currently a Distinguished

Professor and Dean of Research & Development, National Yunlin University of Science and Technology, Taiwan. He is the chair of IEEE Signal Processing Society Tainan Chapter, and an Associate Editor of the *International Journal of Control Theory and Applications*. His current research interests include neural networks and their application to medical image processing, wafer defect inspection, digital watermarking, and pattern recognition. In the above areas, he has more than 150 publications in journals and conference proceedings.

He was a member of the organization and program committees for more than 50 times, organized and chaired for more than 30 technical sessions for many international conferences. He is a Life Member of IPPR and the Taiwanese Association for Artificial Intelligence (TAAI), senior Member of IEEE, and is listed in *Who's Who in the World*, *Who's Who in Science and Engineering*, *Who's Who in Asia*, and *Who's Who of Emerging Leaders*.

Yi-Feng Lin received the B.S. and M.S. degree in 2009 and 2012, respectively, from the Department of Computer Science and Information Engineering, National Yunlin University, Yunlin, Taiwan. His research interests include neural networks, digital image processing and their applications.